Backward positive pion production from nuclei bombarded with 600 MeV protons, 700 MeV alpha particles, and 350 MeV deuterons

C. F. Perdrisat
Department of Physics, College of William and Mary, Williamsburg, Virginia 23185

S. Frankel and W. Frati
Department of Physics, University of Pennsylvania, Philadelphia, Pennsylvania 19104
(Received 26 April 1978)

The momentum dependence, at fixed pion angles of 180 and 155°, of inclusive pion production reactions has been obtained for 600 MeV protons and 175 MeV/nucleon α particles and deuterons on ^{6}Li, C, Co, and Ta. The spectra obtained all fall off exponentially with increasing pion momentum, the slope being about 30 MeV/c independent of either target or projectile nature. The data are examined from the point of view of quasi-two-body scaling, a reaction description discussed recently which suggests that $q_{\min}$, the minimum nuclear recoil momentum possible kinematically, is the proper scaling variable. When plotted versus $q_{\min}$, all data presented here keep their exponential shape, but the slope becomes 70 MeV/c, i.e., nearly the same as obtained for proton production by the same selection of beam projectiles and energies. It is concluded that the same functional of the target momentum space wave function is revealed by quasi-two-body scaling in inclusive pion production experiments, as in inclusive proton and light-fragment production experiments. Finally, the results of a Monte Carlo calculation of pion spectra based on a single $NN \rightarrow \pi NN$ interaction and taking into account the internal motion of the nucleons in target and projectile are presented. The shape and cross sections are accounted for when effective momentum densities of exponential forms are used; the slope constants necessary are compatible with the ones obtained in quasi-two-body scaling. Using the ground state momentum density of an independent particle shell model produces pion spectra which fall off too rapidly. Furthermore, the Monte Carlo calculation reveals kinematical features of the reaction, which help explain why quasi-two-body scaling works for pion production.

[NUCLEAR REACTIONS C(p,π), E_p=600 MeV, (d,π), E_d=350 MeV, (α,π) E_α =700 MeV; ^{6}Li, Co, and Ta(d,π), E_d=350 MeV, (α,π), E_α=700 MeV; measured $\sigma(E_\pi,\Theta_\pi)$ at 155 and 180°; magnetic spectrometer; compared with quasi-two-body scaling and Monte Carlo, single interaction calculation; discuss relation to internal motion in target and projectile.]

I. INTRODUCTION

Positive pion production in the collision of a proton with hydrogen requires a minimum beam energy of 292 MeV. However, on the moving nucleons of a nuclear target, pion production can occur at lower beam energy, as long as the incident projectile has a kinetic energy larger than the pion rest mass. Thus the study of pion production below 300 MeV on nuclear targets tests both existing nuclear wave functions and description of the pion production mechanism.

Besides the original pion production work with 390 MeV α particles at Berkeley,[1] relatively little experimental data exist so far: The largest number of experiments has been carried out with 185 MeV protons by the Uppsala group,[2] and there are preliminary data at 154 and 164 MeV from the Indiana cyclotron[3]; an experiment with 154 MeV protons has been reported by the Orsay group,[4] and one with 200 MeV polarized protons by a TRIUMF group.[5] All these experiments but the first one were studies of exclusive cross sections to definite final states of the residual nucleus. The only experiment with complex projectiles is that of Wahl *et al.*,[6] who have investigated inclusive π^0's production by 180 MeV and 200 MeV ^{3}He on carbon, 200 MeV ^{3}He on lead, and 710 MeV α particles on carbon. In these experiments the π^0's were identified from the annihilation γ rays in coincidence at symmetric angles up to 90°; thus these data pertain mostly to forward pion production.

The experiment to be reported here was a measurement of inclusive cross sections $d\sigma^3/d\Omega_\pi dp_\pi$ as a function of pion momentum p_π, for pions emitted at 180 and 155° in the laboratory. Four targets were investigated: ^{6}Li, C, Co, and Ta; the beams were 600 MeV protons, 700 MeV α particles, and 350 MeV deuterons. Inclusive (p,π) reactions had been investigated earlier by Cochran *et al.*[7] at 730 MeV, at angles extending up to 150° for Be, C, Al, Cu, and Pb, as well as by James *et al.*[8] for Be, C, Cu, and Pb at 600 MeV up to 150°.

The experiment is described in Sec. II, and the data are given in a table and graphical form in Sec. III. In Sec. IV it is demonstrated that the data scale like the proton production data, when the variable $q_{\min}$ of quasi-two-body scaling is used in-

stead of the observed pion momentum p_π. Finally, Sec. V presents the results of a Monte Carlo calculation for the reaction; it also describes the method use to extract appropriate "effective" momentum distributions for both projectile and target for use in the Monte Carlo calculation. The conclusions are presented in Sec. VI.

II. DESCRIPTION OF THE EXPERIMENT

The experiment was performed with beams of 600 MeV protons, 700 MeV α particles, and 350 MeV deuterons at the Space Radiation Effects Laboratory in Newport News.[9] The apparatus was the same as that used to study the 180° production of protons by the same particles at the same energies.[10] Figure 1 shows the layout. The beam reached the target located downstream of the dipole magnet; backward emitted pions were bent by the dipole and focused on scintillator $S2$ by the quadrupole doublet. Counters $S1$, $S2$, and $S3$ were part of a coincidence telescope and located inside a lead shielded tunnel necessary to decrease room background. The counters were the same as described in Ref. 10.

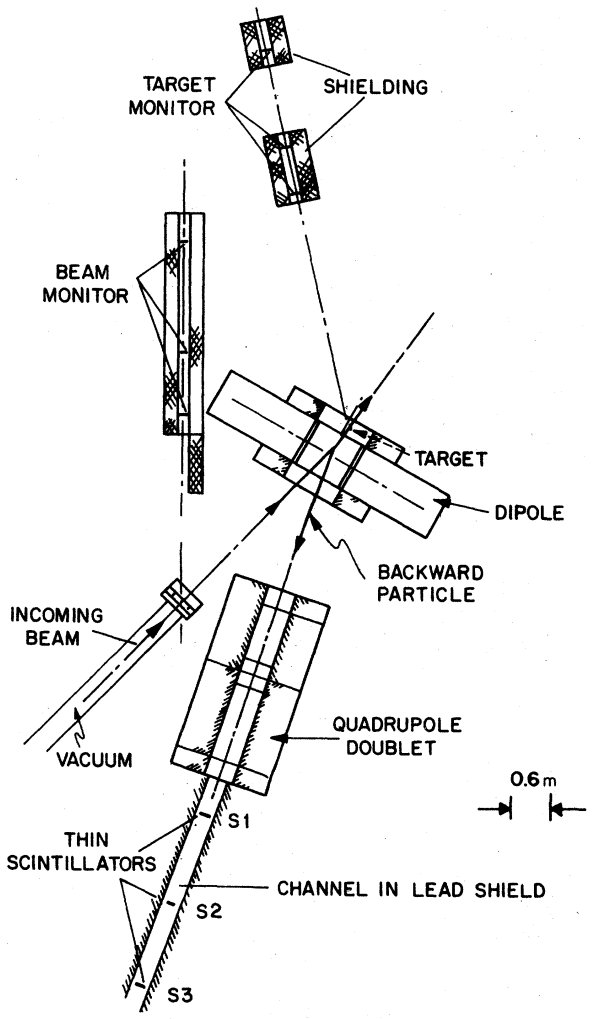

FIG. 1. Floor plan of the experimental setup used in the present study.

Times-of-flight between the different counters were digitized and fed into an on-line computer, together with pulse heights from all three counters. For 180° pions, the momentum was selected by varying the dipole and quadrupole fields. The tuning calculated by ray tracing has been verified with a floating wire measurement. For 155° pions the dipole was turned off and the quadrupoles provided the momentum selection. In the time-of-flight spectra the pions were well separated from other charged particles, largely because for the momentum range of interest (80 to 200 MeV/c for the α particle and deuteron beams), the stopping range of nucleons or light fragments of the same momentum was significantly smaller than the target thickness. Figure 2 shows a typical time-of-flight spectrum for $C(\alpha, \pi)$ for 180° pions of 120 MeV/c and one for $Ta(\alpha, \pi)$ for 155° and the same momentum.

The targets used were ^{6}Li (790 mg cm^{-2}, enriched to 96% in ^{6}Li), C (730 mg cm^{-2} of graphite), Co (1130 mg cm^{-2} metal), and Ta (840 mg cm^{-2} metal). Relative beam rates were monitored with two independent three-counter telescopes, one viewing a thin radiator upstream from the experiment, and the other viewing the target. Absolute rates were obtained from carbon activation, comparing the β^+ annihilation γ rate from the ^{11}C produced with that

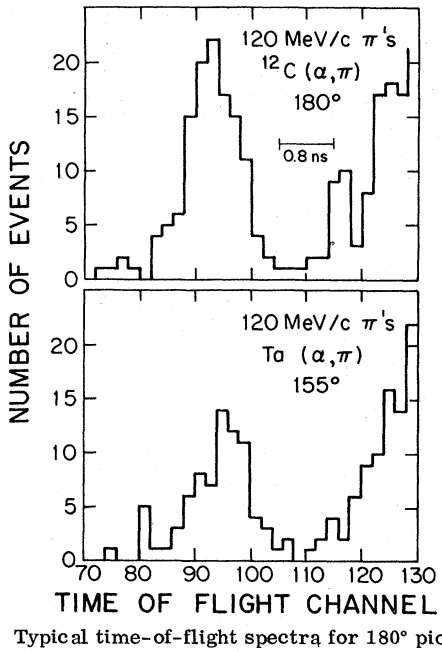

FIG. 2. Typical time-of-flight spectra for 180° pions in $C(\alpha, \pi)$ and 155° pions in $Ta(\alpha, \pi)$; in both cases the average pion momentum was 120 MeV/c.

of a calibrated ^{22}Na source. The activation cross section for 600 MeV protons is well known; a value of 30.5 ± 0.6 mb was used.[11] For the activation by 700 MeV α particles, a value of 50 ± 4 mb was taken from Dollhopf.[12] Since no experimental cross section is known for the ^{11}C activation from 350 MeV deuterons, a value of 60 mb was used, based on the systematics of lower energy measurements; the uncertainty on the latter could be as large as ±50%.

III. DATA AND CROSS SECTIONS

The number of pions per monitor count was obtained from the time-of-flight spectra at appropriate settings of the currents in the magnets. As shown in Fig. 2, the time-of-flight spectra have an easily identifiable peak at the position expected from the momentum selection, with a few events corresponding to velocity c, and an important continuum of slower particles on the right. It was sometimes necessary to subtract a background under the pion peak, but for most of the data this correction amounted to less than 20% of the counts in the peak.

The raw data were corrected for decay-in-flight of the pions. Due to the large target-to-detector distance (6 m), the small size of the counters, and the angular distribution of the decay muons (the Jacobian angle was typically 10 times larger than the angular acceptance) the decay correction was close to the maximum corresponding to a survival probability of $\exp(-1.28\times10^{-3}d/\gamma\beta)$, with d in cm the distance from the target to the focal plane detector. The final correction applied did take into account the probability that the muon would stay within the solid angle, as well as the geometry of the three-counter telescope. The smallest survival probability was 26% at 80 MeV/c, and the largest 88% at 400 MeV/c. No correction was applied for multiple Coulomb scattering in the targets or in the helium placed between the target and the first detector in the telescope. The target correction was negligible because the typical root-mean-square Coulomb angle for 100 MeV/c pions was typically 1.4° (for the carbon target), and the angular dependence of the measured cross section is weak, as will be seen below.

A correction for energy loss in the different targets was obtained by multiplying the specific energy loss at each pion energy by the half-target thickness. The pion momenta in Table I reflect this correction. The data were also corrected in first order for the finite momentum resolution of the spectrometer; an effective momentum was obtained for each point assuming the resolution profile to be Gaussian and the pion spectrum to be exponential; as will be seen below, the latter assumption is well borne out by the data. The resolution correction is significant for the (p,π) data, but not for the (d,π) and (α,π) data, because the latter extend only to 200 MeV/c. Again, the data in Table I reflect this correction.

In Table I the data are given in the form of differential cross sections $d\sigma^3/d\Omega_\pi dp_\pi$, with relative statistical error. The systematic errors due to calibration of the beam intensity, absorption and multiple scattering in the targets, and along the flight path are estimated to be ±20% for the proton data, ±25% for the α particle data, and 55% for the deuteron data. However, the systematic errors on the relative cross section for a given beam should be less than 10% for all targets and for any given pion momentum. The momentum itself is defined within ±1%, and the full width at half maximum is ±7.5% based on the analysis in Ref. 10. The data for C(p,π) at 600 MeV and 155°, and ^{6}Li, C, Co, Ta (α,π) at 700 MeV and 180° [also shown is Ta(α,π) at 155°] are shown in Fig. 3, where the cross sections $d^3\sigma/d\Omega_\pi dp_\pi$ are plotted versus the laboratory pion momentum. Also shown are the C(p,π) data of Cochran *et al.* (Ref. 7) taken at 730 MeV and 150°; the agreement between the two sets of (p,π) data for carbon is reasonable, taking into account the different energies for these two experiments, and the systematic errors in each. Also shown are three data points for C(p,π) at 600 MeV and 150° from James *et al.* (Ref. 8). Comparing the 730 MeV (p,π) data with the 700 MeV (α,π) data for carbon immediately shows that the α particles does not behave like a structureless particle in the process: The ratio of these two cross sections is about 1300, although the beam energies are nearly the same. Worth pointing out also, is the similarity in shape for all (α,π) data; the shape in all cases is nearly exponential, with a slope of 30 MeV/c. The apparent target dependence is close to A^1, with the exception of ^{6}Li. It is important to note that the A dependence of the (α,π) data is quite different from the A dependence found experimentally in backward inclusive proton production (p,p) in Ref. 13: The pion data presented here show an A^1 dependence when represented as a function of the *measured* pion momentum; but in Ref. 13 the (p,p) data did not show a similarity in shape nor a simple A dependence when plotted as a function of the observed proton momentum. This important point will be discussed in Sec. IV.

Table I includes data points for C(d,π) at 350 MeV, at 180° and 155°; the absolute normalization of the latter is in doubt by a factor of 2, although the slope is correct. The ratios of cross sections for a given target such as carbon, and incident protons, deuterons, and α particles are remarkable; for example, for 150 MeV/c pions these ratios are (p,π) 600 MeV/(α,π) 700 MeV/(d,π) 350 MeV = 1200/

1/0.08. As will be discussed in Sec. V, these ratios can be explained in terms of the structure of the α particle and deuteron projectiles, assuming that the pion producing process is $pp \to np\pi^+$.

IV. SINGLE INTERACTION PICTURE AND QUASI-TWO-BODY SCALING

Recent studies of the backward production of protons and other light fragments by incident protons and other projectiles have demonstrated the existence of an empirical scaling law (see Refs. 10, 14, and 15). When represented as a function of a recoil variable $q_{\min}$ to be defined below, the inclusive cross section $d^3\sigma/d\Omega p^2 dp$ takes a nearly exponential shape, with a slope constant q_0 which is approximately independent of the projectile's nature and energy, of the fragment observed, as well as of the angle of emission, as long as the latter is in

TABLE I. The cross section $d^3\sigma/d\Omega_\pi dp_\pi$ obtained in the present experiment; the pion momenta p_π have been corrected for target energy loss and resolution, as described in the text.

p_π (MeV/c)	$d^3\sigma/d\Omega dp_\pi$ cm^2 sr^{-1} (GeV/c)$^{-1}$	% error
	600 MeV protons on carbon, 155°	
88	6.47 (-27)	2.7
97.5	6.95	2.3
103	7.9	2.7
112.5	8.54	1.6
132	9.49	1.5
152	6.51	1.7
178.2	4.31	1.6
197.3	2.52	2.2
220.7	1.46	3.8
244.2	5.75 (-28)	4.8
267.8	2.69	6.6
290.5	1.31	6.0
336.8	4.8 (-29)	31
382.5	1.1	38
	350 MeV deuterons on carbon, 180°	
101.5	3.61 (-30)	13
129.5	9.17 (-31)	10
	350 MeV deuterons on carbon, 155°	
91	8.36 (-30)	9.8
109	1.17 (-29)	8.1
127	8.03 (-30)	8.4
136	5.62	9
146	4.55	9
155	2.51	7.7
164	1.85	6.0
	700 MeV α particles on ^{6}Li, 180°	
101.2	2.99 (-30)	10.4
120	2.57	12.5
139.4	1.42	13.2
158.6	7.26 (-31)	14.9
177.8	4.28	17.4
	700 MeV α particles on carbon, 180°	
101.7	1.52 (-29)	2.8
110.5	1.51	2.7
120	1.28	2.0
129.7	9.12 (-30)	2.8
139.4	7.57	1.7
149	5.18	2.3
158.6	4.82	1.7
168.2	2.68	1.9
177.8	1.91	1.5
196.8	9.41 (-31)	1.0
	700 MeV α particles on cobalt, 180°	
84.5	7.26 (-29)	10.5
101.7	5.62	8.4
120.5	4.53	8.8
139.4	3.58	9.5
159.1	1.73	11.5
177.8	9.32 (-30)	12.1
196.8	5.43	12.5
	700 MeV α particles on tantalum, 180°	
102	1.17 (-28)	12.7
119.5	1.52	11.5
138.4	8.24 (-29)	11.9
148	5.74	15.4
157.6	4.91	11.6
167.6	4.20	14.4
176.8	2.01	21.3
	700 MeV α particles on tantalum, 155°	
85.2	4.14 (-28)	11
91	3.86	11.9
100.7	3.15	12.7
110	2.82	8.3
119.5	2.50	12.1
128.7	2.43	10.9
138.4	1.29	14.9
148	1.16	8
157.6	8.62 (-29)	10
167.2	6.01	7.1
176.8	4.14	10.8
195.8	1.59	17.7

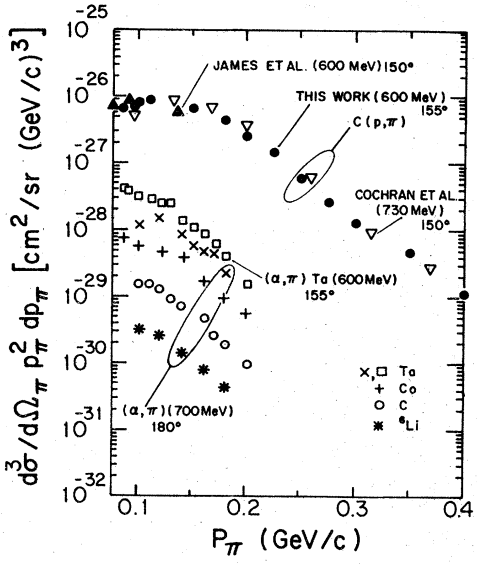

FIG. 3. Inclusive cross section $d^3\sigma/d\Omega_\pi dp_\pi$ vs laboratory pion momentum for (p,π) at 155° and for 600 MeV protons on carbon, shown as ●, and (α,π) for 180° and 700 MeV α particles on ^{6}Li(*), C(⊙), Co(+), and Ta(×); also shown are data points for Ta(α,π) at 155°(□). The 730 MeV proton data of Cochran *et al.* (Ref. 7) and the 600 MeV proton data of James *et al.* (Ref. 8) are also shown for comparison as (△) and (▲), respectively; both distributions are for 150° pions and carbon.

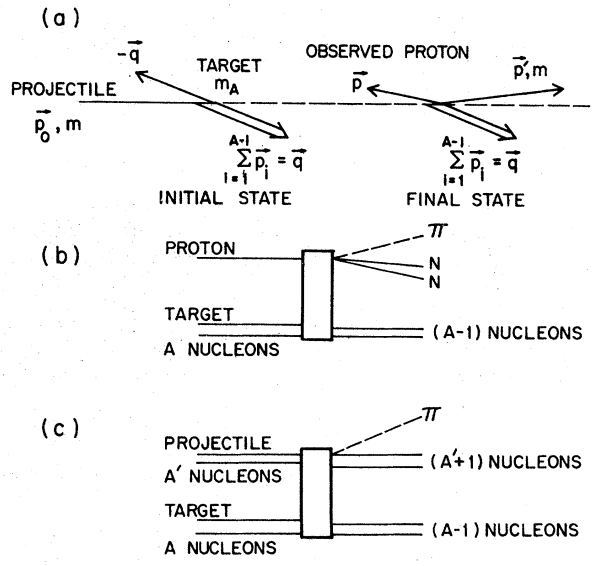

FIG. 4. (a) Kinematics for quasi-two-body scaling discussed in Sec. IV, as it applies to backward proton emission. (b) Final state in the production of one pion by a proton incoming on a complex nucleus of atomic number A. (c) Final state postulated in the modified quasi-two-body scaling for backward pion emission.

the backward hemisphere. Furthermore, for proton emission and incident protons of several hundreds of MeV's, the magnitude of the cross section goes like A, the atomic number of the target. This scaling law reduces a very large body of inclusive data to a few parameters; to what extent the $q_{\min}$-variable parametrization reveals the internal momentum wave function of the target is a question which has not been entirely resolved yet. However, one interpretation which has been discussed elsewhere (see Refs. above) will be discussed here briefly, to facilitate its adaptation to the pion emission case.

For backward proton emission, the angle at which the proton is detected cannot be reached in a single nucleon-nucleon interaction if the target nucleon is at rest. Of several possible starting assumptions, the point of view is taken here that the observed particle is not the projectile, but rather a constituent of the target; this is the first assumption. A second assumption is that the observed particle or fragment was freed from the target in a single interaction, with low momentum transfer. A third assumption is that no large momentum transfer to the rest of the target occurred either, so that the residues of the target move forward with small relative momenta between its constituents, and small excitation; thus no other fast fragment but the scattered projectile is expected in the forward direction. The kinematics corresponding to the model thus defined is illustrated in Fig. 4(a), which is specialized to an incident proton and an observed backward proton.

In the picture just outlined, the observed momentum $\vec{p}$ cannot be very different from the internal momentum $-\vec{q}$ of the target proton because the momentum transfer is assumed to be small. The obvious conclusion is that the momentum spectrum of the observed particle is connected in some way to the internal momentum wave function of the target in this model. If the functional relation between the observed momentum distribution and the internal momentum wave function preserve the rapid decrease of the latter with increasing recoil momentum q, the minimum kinematically possible recoil $q_{\min}$ may suffice to characterize the data. It is this observation which led to the idea of quasi-two-body scaling (QTBS) for inclusive backward production data: Inclusive cross sections $d^3\sigma$ displayed as a function of $q_{\min}$ do scale.

Using the parameters defined in Fig. 4(a), conservation of momentum and energy gives

$$\vec{p}_0 = \vec{p} + \vec{p}' + (\Sigma \vec{p}_i)$$

and

$$E_0 = E_p + E_{p'} + (\Sigma E_i) - m_A ,$$

which can be rewritten, so as to make appear the quasi-two-body nature of that part of the final state which is not observed, as follows:

$$\vec{P}=\vec{p}_0-\vec{p}=\vec{p}'+\vec{q},$$

$$\epsilon=E_0-E_p+m_A=E_{p'}+E_q,$$

where $\vec{q}=(\Sigma\vec{p}_i)$ and $E_q=(\Sigma E_i)$ are the recoil momentum and energy of the residueal $(A-1)$ nucleons of invariant mass $M^2=E_q^2-q^2$. For fixed values of $\vec{P}$ and ϵ, $\vec{q}$ is minimum when $\vec{p}'$ and $\vec{q}$ are collinear. The value of this minimum q is

$$q_{\min}=\frac{1}{2(\epsilon^2-P^2)}\{P(\epsilon^2-P^2-m^2+M^2) - \epsilon[(\epsilon^2-P^2-m^2-M^2)^2-4m^2M^2]^{1/2}\}, \quad (1)$$

where m is the nucleon mass. In Eq. (1), $q_{\min}$ is a function of the invariant mass M of the residual $(A-1)$ nucleon system; $q_{\min}$ decreases when M decreases. As the smallest possible invariant mass M occurs when the $(A-1)$ nucleons are in their ground state, one may take $M=m_{A-1}$.

The minimum recoil $q_{\min}$ defined in (1) has been called the quasi-two-body scaling variable, because it has been obtained from the assumption that the unobserved, forward going reaction residues were only two in number, the scattered projectile and the remainder of the target in a state of low excitation. Essentially identical arguments will now be used to define a QTBS variable for pion production, for which the elementary process is presumably

$$NN\rightarrow\pi NN. \quad (2)$$

If only the pion is observed, at least three other particles must be in the forward region: The two nucleons involved in reaction (2) and the residues of the target, as illustrated in Fig. 4(b). In the spirit of the definition of $q_{\min}$ discussed above for nucleon production, it will be assumed that $q_{\min}$ must be calculated for the minimum invariant mass of the two nucleons involved in reaction (2). The picture can then easily be extended to a complex projectile of atomic mass A': $q_{\min}$ will occur when $(A'+1)$ nucleons have the smallest possible invariant mass; in this case again, the final state is thus reduced to a quasi-two-body one for the unobserved fragments. As will be shown shortly the definition of the QTBS variable just presented, leads to the same scaling for pion production, as has been found for nucleon production.

The expression for $q_{\min}$ is easily obtained from (1), if one redefines $\vec{P}$ and ϵ as

$$\vec{P}=\vec{p}_0-\vec{\pi}=\vec{p}'+\vec{q}$$

and

$$\epsilon=E_0+m_A-E_\pi=E_{p'}+E_q,$$

where now $\vec{p}'$ is the momentum of the $(A'+1)$ system, $\vec{q}$ is that of the $(A-1)$ target fragments. Equation (1) can then be used to calculate $q_{\min}$ simply replacing m by $m_{A'+1}$, the invariant mass of the projectile-plus-one-nucleon system. For an incident proton, $\ldots m_{A'+1}\sim m_d$, the mass of the deuteron; for an incident deuteron, $\ldots m_{A'+1}\sim m_t$, the mass of a triton; finally for an incident α particle, the value $m_{A'+1}\sim m_{^4\mathrm{He}}+m_n$ must be taken, as the five-nucleon system has no bound state.

The inclusive pion cross sections $d^3\sigma/d\Omega_\pi p_\pi^2 dp_\pi$ for carbon and incident protons, deuterons, and α particles obtained in the present experiment are shown in Fig. 5, plotted as a function of $q_{\min}$. On the same figure, the results of Ref. 10 for proton emission, for the same three beam particles and again carbon as a target, are also shown; the semilogarithmic representation linearizes the data, and the slopes are very similar in all cases. Note that the (p,π) data are for 155° pions; all other data are for 180° emission, but for (d,π) which is available at both angles. A common slope for all seven groups of data points is 68 MeV/c. Only the two points for the largest $q_{\min}$ values in C(p,π) de-

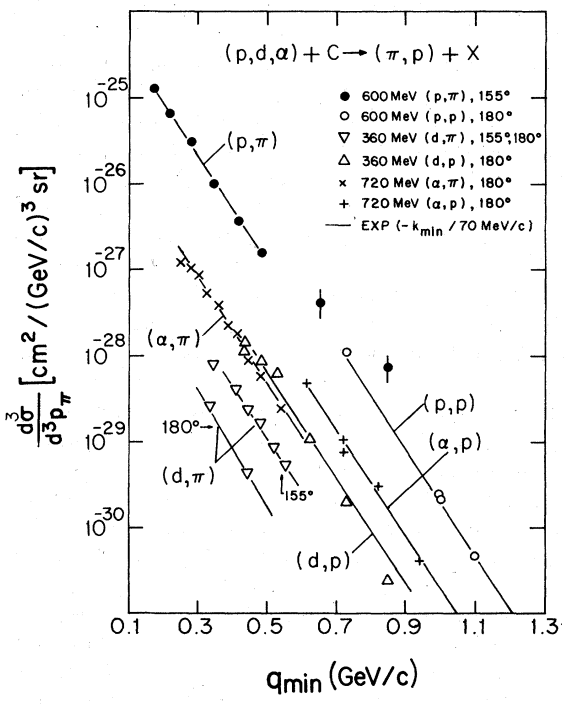

FIG. 5. Inclusive cross section $d^3\sigma/d\Omega_\pi p_\pi{}^2 dp_\pi$ vs minimum recoil $q_{\min}$ for C(p,π), C(α,π), and C(d,π), compared with results of Ref. 10 for C(p,p), C(α,p), and C(d,p). The p, α, and d energies are the same in the π- and p-production data.

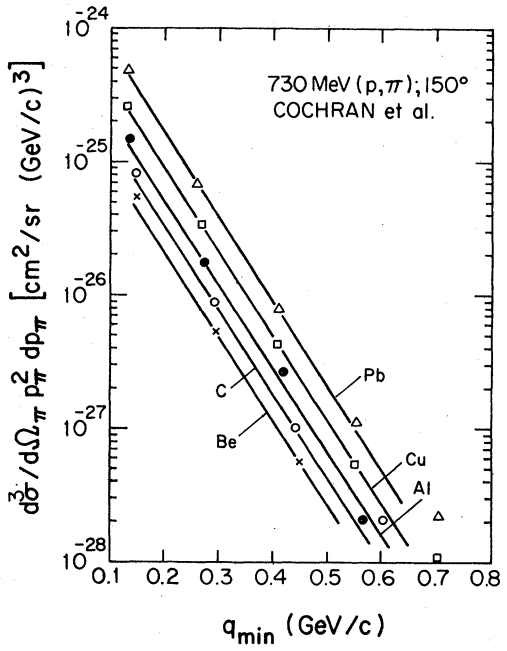

FIG. 6. Results of Cochran *et al.* (Ref. 7) for 730 MeV protons, pions at 150° represented vs q_{min}. The straight lines have a slope of 68 MeV/c and are only eyeball fits. The (×) are for Be, (o) for C, (·) for Al, ( ) for Cu, and (△) for Pb.

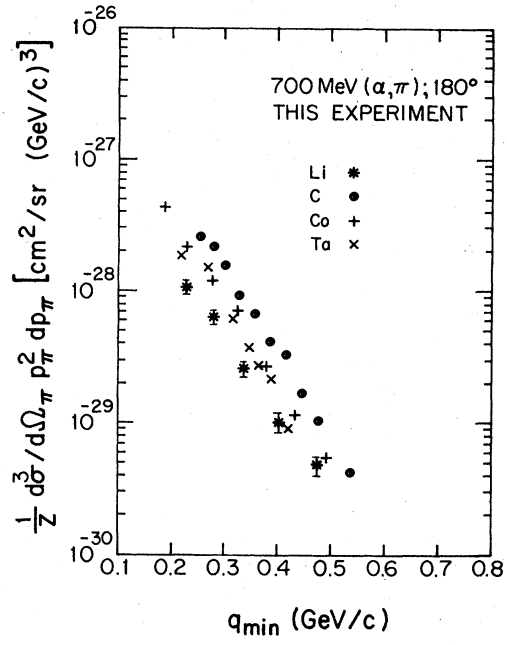

FIG. 7. Inclusive cross section $d^3\sigma/d\Omega_\pi p_\pi{}^2 dp_\pi$ multiplied by $(1/Z)$ as a function of q_{min} for (α,π) on ^{6}Li(*), C(o), Co(+), and Ta(×), for 155° pions and 700 MeV α particles.

viate markedly from the universal exponential behavior. This representation of the π- and proton-inclusive cross sections shows the same scaling for both channels and for three different beam particles, and thus indicates that the pions reveal the same functional of the target momentum space wave function as the protons.

For comparison, the 150° (p,π) data of Cochran *et al.* (Ref. 7), which are for 730 MeV protons, are shown in Fig. 6. A comparison with Fig. 5 shows immediately that the slopes are the same for targets from Be to Pb. Finally, in Fig. 7, the (α,π) data from the present experiment are shown vs. q_{min}; however, to explore the target dependence, in this case the cross sections have been divided by Z, the number of protons in the target nuclei. Because for π^+ production, the protons in the target are expected to contribute most of the cross section, Z rather than A has been chosen. An approximate fit to the data in Fig. 7 gives $Z^{0.6}$ if one does not include ^{6}Li. Similarily, the Cochran *et al.* (p,π) data in Fig. 6 give $Z^{0.55}$ if one does not include ^{9}Be. In both sets of data, the lightest target has a distinctly smaller cross section than expected on the basis of the Z dependence observed for the heavier ones; however, no noticeable difference in slope is found for the lightest targets.

The target dependence obtained here is quite different from the one obtained by plotting the data vs the observed pion momentum p_π, which has been found to be A, rather than $Z^{0.6}$ in Sec. III above. In Ref. 7, Cochran *et al.* had pointed out that the angle- and energy-integrated cross section σ_T^π varied like $Z^{1/3}$ for targets heavier than carbon. The result of the scaling transformation from p_π to q_{min} is thus to change the apparent Z dependence from $Z^{1/3}$ to $Z^{0.55}$. This conclusion is quite different from the one obtained for proton production, where an A dependence is the rule when the QTBS variable is used, whereas no simple A dependence can be found when the observed proton momentum is used instead. This difference in target dependence must be related to the different absorptions of pions and protons in nuclear matter, as it is observed both with proton and α particle projectiles. Cochran *et al.* had observed that the ratio $(d^3\sigma/d\Omega_\pi dE_\pi)/\sigma_T^\pi$ was largely target independent, thus indicating a very similar angular and energy dependence for all pion spectra; this point is made much stronger with the representation in Fig. 6 which emphasizes the identical shapes obtained with the QTBS variable q_{min}.

V. MONTE CARLO SIMULATION OF PION PRODUCTION

In the preceding section, the data have been analyzed in terms of the recoil variable q_{min}, which is

relevant in QTBS. In the present section, pion spectra will be calculated by a Monte Carlo technique, assuming that the basic interaction is $NN \rightarrow \pi NN$ and taking the structure of both target and projectile explicitly into account.

If one assumes that the basic, pion producing interaction is $NN \rightarrow \pi NN$ rather than coherent nucleus-nucleus interaction, then pion production by 700 MeV α particles or 350 MeV deuterons is below threshold; in both cases the energy per nucleon in the projectile is 175 MeV, whereas the minimum energy required in a nucleon-nucleon collision is 292 MeV if the target nucleon is at rest. In this case, pion production can only occur with the help of internal motion in the target and in the projectile. A 175 MeV proton can produce a pion in a collision with a 25 MeV (momentum 220 MeV/c) target proton moving in a direction opposite that of the beam particle, a head-on collision. Internal momentum in complex projectiles of course reduces this minimum requirement.

The calculation requires the probability for the target and projectile nucleons to have given internal momenta. For the target nucleon, it is not the ground state distribution that enters; orthogonality of the target and continuum final states has been shown in Ref. 15 to result in a cancellation by final state interactions. Thus an "effective" momentum distribution must be used, with a normalization determined here from the C(p, π) data. The shape of this "effective" distribution was taken of the form

$$(1/q)^n \exp(-q/q_0), \quad \text{with } n=1. \tag{3}$$

This form has been shown in Ref. 14(c) to lead to an exponential falloff of the inclusive cross section in (p,p), within the framework of the model which has been succintly described in Sec. IV above.

For the projectile, no cancellation occurs, and the normalization of the distribution is equal to the number of participating projectile nucleons; distortion effects are expected but not included here. The projectile distribution was also taken of form (3), but the results of the calculation are not sensitive to the power n; $n=0$ or 2 produces similar results for slightly different values of q_0.

The model assumed for the Monte Carlo calculation will now be described step by step. Consider the interaction of two complex nuclei, such as α particle and C nucleus. First, it is assumed that the projectile containing A' nucleons and having mass $m_{A'}$ fragments into a residual system of $(A'-1)$ nucleons and a proton of momentum $\vec{q}_p$ relative to the C.M. system of the projectile. The $(A'-1)$ system is on the mass shell, thus the proton has invariant mass squared $m_x^2 = m_{A'}^2 + m_{A'-1}^2 - 2m_{A'}(m_{A'-1}^2 + q_q^2)^{1/2}$; thus $m_x = m_{A'} - m_{A'-1}$ in the limit $q_p = 0$ only. The proton four momentum is then transformed to the laboratory system, where it has then four momentum

$$(\vec{p}_p, E_p) = \gamma(\vec{q}_p + \vec{\beta}E_q, \vec{\beta}\cdot\vec{q}_p + E_q);$$

$\vec{\beta}, \gamma$ are the Lorentz factors of the initial projectile with beam momentum $\vec{p}_0$, and energy E_0:

$$\vec{\beta} = \vec{p}_0/E_0, \quad \gamma = E_0/m_{A'}.$$

Next, it is assumed that the target nucleus has A nucleons and a mass m_A, and that it fragments into a proton and a residual system of $(A-1)$ nucleons with invariant mass m_{A-1}. The proton has a momentum in the laboratory $\vec{q}_t$, but its mass is less than its physical mass even for $q_t = 0$ because $m_A - m_{A-1} < m_p$. Following the same scheme as in Sec. IV, it is assumed that both the $(A'-1)$ and the $(A-1)$ residual systems have the smallest possible mass, which are then taken as the ground state masses of these systems. Such final states are favored because they lead to the smallest possible internal momenta q_p and q_t; these are the most likely occurences because the vertex functions rapidly decrease with internal momentum. The total energy squared available at the NN vertex is then given by

$$\begin{aligned} s &= [\vec{p}_p + \vec{q}_t, E_p + m_A - (m_{A-1}^2 + q_t^2)^{1/2}]^2 \\ &= (m_A - m_{A-1})^2 + (E_p^2 - p_p^2) \\ &\quad - 2[\vec{p}_t\cdot\vec{q}_p + (m_A - m_{A-1})E_p - T_R(E_p + m_A)], \end{aligned} \tag{3}$$

where T_R is the kinetic energy of the recoiling $(A-1)$ system given by

$$T_R = (m_{A-1}^2 + q_t^2)^{1/2} - m_{A-1}.$$

Next, pion production in the NN system was assumed to be isotropic, which is a good approximation for πNN final states near threshold. The range of s values playing a role for pion laboratory momenta larger than 100 MeV/c goes from 4.25 to 4.75 GeV^2, whereas the threshold is at $s_0 = (m_p + m_n + m_\pi)^2 = 4.07$ GeV^2, and the (3,3) resonance is at $s = (m_N + m_\Delta)^2 = 4.71$ GeV^2. Over this range the angular distribution should change from isotropic to $(1 + \cos^2\theta_\pi)$; for the small pion angular range of interest here, no visible difference was obtained when the isotropic distribution was replaced by a $(1 + \cos^2\theta_\pi)$ one. In the calculation, each event was assumed to produce a pion if the s value was larger than s_0; a weight factor proportional to the total cross section for single pion production at that value of s was then attributed to each event. Near threshold, the total cross section for πnp final states is given by the empirical relation

$$\sigma_{np\pi^+}(\eta) = 0.95\eta^4 + 0.099\eta^6 + 0.204\eta^8, \tag{4}$$

where η is the pion C.M. momentum in units of the pion rest mass (see for example Lock and Measday[16]). Experimental cross sections are available above 450 MeV. It was observed that both the near-threshold cross section of (4) and the data, where available, were in excellent agreement with three-body phase space, which was then used for the calculation. The pion momentum distribution in the NN C. M. system was assumed to have the three-body phase space form given by Block,[17]

$$d\sigma_3/dp_\pi = \tfrac{2}{3}\pi^2 p^2 \left[1 - \frac{2(m_1^2+m_2^2)}{(\sqrt{s}-E_\pi)^2-p_\pi^2} + \frac{(m_1^2-m_2^2)^2}{[(\sqrt{s}-E_\pi)^2-p_\pi^2]^2}\right]^{1/2} \times \left[3(\sqrt{s}-E_\pi)^2\left(1-\frac{(m_1^2-m_2^2)^2}{[(\sqrt{s}-E_\pi)^2-p_\pi^2]^2}\right) - p_\pi^2\left(1-\frac{2(m_1^2+m_2^2)}{(\sqrt{s}-E_\pi)^2-p_\pi^2}+\frac{(m_1^2-m_2^2)^2}{[(\sqrt{s}-E_\pi)^2-p_\pi^2]^2}\right)\right], \quad (5)$$

where m_1 and m_2 are the physical masses of the two nucleons at the πNN vertex, m_π is that of a pion; p_π, the pion momentum in the NN system, has the maximum value

$$p_\pi^{\max} = \{[s-(m_\pi+m_1+m_2)^2] \times [s-(m_\pi-m_1-m_2)^2]/4s\}^{1/2}.$$

The weight for each event was then taken as

$$w = \int_0^{p_\pi^{\max}} (d\sigma_3/dp_\pi)dp_\pi .$$

Near threshold, πd final states are in fact dominant in pp collisions; however, for the pion laboratory momenta of interest here ($p_\pi > 100$ MeV/c), s is larger than 4.25, and πd final states are decreasingly important with increasing s. Changing from formula (4) to the empirical relation

$$\sigma_{\pi d} = \alpha\eta + \beta\eta^3$$

produced no visible difference in the final result (the latest values of $\alpha = 0.247 \pm 0.017$ and $\beta = 0.6 \pm 0.3$ can be found in Jones[18]; terms in η^2 and η^4, η^5 are neglected here). Neither did the final result change significantly when the three-body phase-space momentum distribution (5) was replaced by two-body kinematics. The latter result is easily understood if one notes that for large laboratory pion momenta directed upstream, a *kinematic* selection occurs anyway, which tends to favor three-body final states with two nearly collinear nucleons; everything else being the same, the resulting pion momentum will be smaller if the two nucleons are not nearly collinear. Also, the three-body phase-space distribution is maximum for nearly collinear nucleons. The higher the pion momentum, the more pronounced this kinematic selection. As a result, the residues of the target and of the projectile, as well as the two nucleons involved in the interaction, all tend to fly nearly parallel to the beam; a condition akin to the assumption of collinearity of the $(A-1)$- and $(A'+1)$ systems in Sec. IV.

Three pairs of angles had to be chosen for each Monte Carlo event: an azimuthal and a polar angle for the orientation of the projectile- and target-internal momentum relative to the beam direction, and for the pion momentum relative to c.m. motion of the NN system. The kinematic selection just mentioned, which is further accentuated by rapidly decreasing effective momentum distributions in both target and projectile, limits the projectile nucleon to a narrow forward cone; likewise, the internal momentum of the target nucleon and the NN c.m. system pion momentum are most likely to be contained within backward narrow cones. The effect of limiting the three polar angles within cones with apertures as small as possible was studied in some detail, as an optimum choice greatly reduces computation time. The final results were obtained with cones of 45° half-aperture for the two internal momenta, and 30° half-aperture for the pion momentum. In the spirit of a Monte Carlo calculation, the internal momenta of the participating nucleons in projectile and target should be chosen according to appropriate momentum distributions. However, because the spectra observed are inclusive, the momentum distributions are not specified. Preliminary analysis indicated that using for these distributions known ground state, independent particle model densities, such as the harmonic oscillator densities with parameters from Elton,[19] failed. As discussed at the beginning of this section, the contribution of the ground state momentum distribution is canceled by final state interactions; an "effective" distribution was used instead, with form (3) and a normalization determined by the $C(p,\pi)$ data. Although no cancellation occurs for the projectile, a distribution of form (3) was also used, but with a normalization determined by the number of participating nucleons in the projectile. No attempt was made to optimize the shape of the distribution for either projectile or target.

Using $q_0 = 70$ MeV/c in (3), the pion spectrum obtained for $C(p,\pi)$ at 600 MeV is shown in Fig. 8. Likewise, for the α particle data on carbon, no agreement could be obtained with a harmonic oscillator helium-4 momentum density. Instead, the

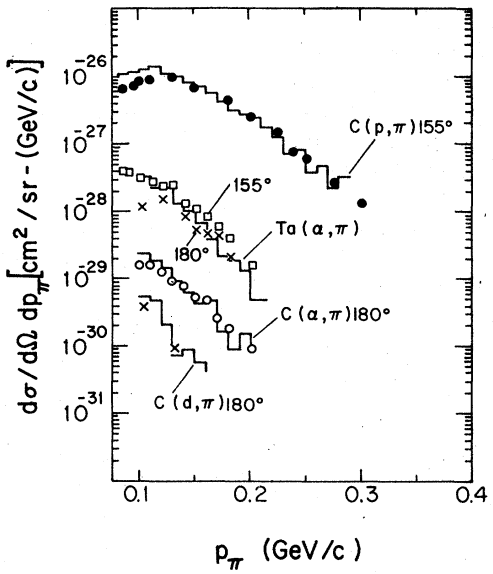

FIG. 8. Histograms of the Monte Carlo results for $C(p,\pi)$, $C(\alpha,\pi)$, and $C(d,\pi)$, normalized approximately to the data for the first of these three reactions. Also shown is the Monte Carlo results for $Ta(\alpha,\pi)$, assuming the target dependence is $Z^{0.6}$. The data points shown are (●) for $C(p,\pi)$, (○) for $C(\alpha,\pi)$, (×) and (□) for $Ta(\alpha,\pi)$ at 180°, respectively, 155°. Also shown are the two data points for $C(d,\pi)$ at 180°(×).

same form (3) was used with a value of q_0 arbitrarily chosen at 90 MeV/c. The result is shown in Fig. 8 again; note that although the $C(p,\pi)$ results are normalized to the data, the $C(\alpha,\pi)$ results necessitated no further normalization other than a factor of 2 for two protons in helium-4. Thus both slope and values of the cross section relative to (p,π) are well reproduced by the calculation. Finally, for the deuteron data, similar results were obtained using either a McGee[20] wave function for the deuteron, or form (3) with $q_0 = 110$ MeV/c; this similarity in the results obtained with the two distributions is not surprising because the McGee momentum distributions is nearly exponential with slope of about 100 MeV/c in the region $300 < q < 400$ MeV/c. The $C(d,\pi)$ results shown in Fig. 8 were obtained with the exponential form; again, no further normalization was necessary, and the slope is in fair agreement with the two data points available. So far then, the calculation explains the large change in cross section observed when carbon is bombarded with different projectiles, as well as the important feature of a unique slope. This is no mean success, if one remembers that the (p,π) reaction is well above threshold for pion production in NN collisions, whereas the (α,π) and (d,π) reactions are below threshold.

In Fig. 8 the results of the Monte Carlo calculation for $Ta(\alpha,\pi)$ are also shown. Again, the effective momentum density (3) was used for the target, with $q_0 = 70$ MeV/c. The number of nucleons in the target participating in the reaction was taken as $Z^{0.6}$, in agreement with the results in Sec. IV. That the cross section should depend upon Z rather than A is suggested by the ratio of the cross sections for π^+ production in pp and np reactions, which is approximately 5 to 1. The power of 0.6 required to normalize the Monte Carlo result to the Ta data is representative of the strong absorption of the outgoing pions; it is in agreement with the findings in Sec. IV, and in definite contrast with the results for the (p,p) inclusive channel. A number of calculations of inclusive pion spectra have been reported earlier. A few will be mentioned here; their emphasis was usually different from the one which motivated the present study. For example, Sternheim and Silbar[21] succeeded quite well in reproducing the 730 MeV data of Cochran *et al.* (Ref. 7) at forward pion angles, using the isobar model and a semiclassical description of the traversal of the nucleus by proton and pion. However, for the largest pion angle considered in Ref. 21 (150°), the calculated spectrum reaches zero at 100 MeV (200 MeV/c), whereas the data show measurable cross sections up to 350 MeV (400 MeV/c). The same basic assumption are used in Ref. 21 as in the Monte Carlo calculation presented here; however, in Ref. 21 charge exchange and absorption of the outgoing pions have been taken into account; on the other hand Fermi motion was neglected which is the essential ingredient for pion production near threshold.

Similarly, Harp[22] has studied single pion production using the isobar model in an intranuclear cascade calculation. Again the results underestimate the high momentum tail observed at 150° in the data of Cochran *et al.*,[7] as well as in the present experiment.

One attempt to calculate pion production below threshold has been reported by Bertsch[23] for heavy ion collisions. Bertsch attributes pion production near threshold to a combination of projectile- and target-Fermi motion, as done here, but he expects that the initial distribution rapidly gets thermalized while the two nuclei penetrate each other, strongly suppressing pion production; however, he considers only heavy ion collisions in which the momentum is in the range 100 to 300 MeV/c per nucleon, to be compared with 600 MeV/c for the present data.

VI. CONCLUSIONS

The back angle pion spectra obtained in the present experiment for the inclusive reaction (p,π) at

600 MeV have been discussed. Using data from Ref. 7, it has been shown that the shape of these spectra was independent of the nature of the target. The same shape was also observed for the pion spectra produced by 700 MeV α particles and 350 MeV deuterons, although the cross sections are three and four orders of magnitude smaller than the (p, π) ones. A very similar conclusion had been previously obtained (Ref. 10) for backward proton spectra from the inclusive reaction (p,p) and also (α,p) and (d,p). The latter observation had been related to quasi-two-body scaling which obtains in a single scattering model and has been discussed in Refs. 10, 14, and 15. In the present work, QTBS has been modified to take into account the presence of the pion in the final state. The application of the modified QTBS has now been found to result in the same universal, exponential behavior of the cross sections for pion production as for proton production by p-, d-, and α-beam particles; this result is best demonstrated in Fig. 5.

One of the important assumptions of QTBS is that final states with minimum relative kinetic energies between the constituents of the fragments dominate the process; this assumption has been studied here, using a Monte Carlo calculation of the single scattering process. The calculation gave excellent agreement for the shape and relative magnitudes for the carbon cross sections for (p, π), (d, π), and (α, π). The effective internal momentum distributions which were found necessary to achieve this agreement were of exponential form, with slope constants of 70 MeV/c for carbon, 90 MeV/c for the α particle, and 110 MeV/c for the deuteron. The calculations also show that for backward pion production, the kinematic constraints imposed by energy and momentum conservation result in restrictions of the phase spaces available to target- and projectile-nucleons participating, and in the region of phase space the pion can reach. This restriction is exactly of the same nature as the QTBS assumption that the final state most likely contains the target minus one nucleon, and the projectile plus one nucleon, both in states of minimum internal excitation. The agreement between the simple Monte Carlo calculation presented and the data may be in part accidental, and certainly will require further testing. The shape of the calculated pion spectrum depends upon a delicate balance of at least three rapidly varying functions: The rapidly decreasing nucleon wave function in the projectile and in the target and the rapidly increasing pion-production cross section. Data for (p, π) near threshold (in the range 185 to 250 MeV), and (α, π) well above threshold (2–4 GeV), would provide very severe tests of the results presented here.

ACKNOWLEDGMENTS

We would like to thank the Space Radiation Effects Laboratory staff for its great dedication during the experiment, and Professor H. Brody, as well as Mr. D. Yang and Mr. D. L. Scherer for help with the data taking. This work was supported in part by the U. S. Department of Energy.

[1]E. Gardner and C. M. G. Lattes, Phys. Rev. 74, 1236A (1948).
[2]S. Dahlgren, B. Hoistad, and P. Grafstrom, Phys. Rev. B 35, 219 (1971).
[3]A. D. Bacher *et al.*, in the Abstract of the Conference Proceedings to the Seventh International Conference on High Energy Physics and Nuclear Structure, Zurich, 1977 (unpublished), p. 28; see also R. D. Bent *et al.*, *ibid.* p. 14.
[4]Y. Le Bornec, B. Tatischeff, L. Bimbot, I. Brissaud, J. P. Garron, H. D. Holmgren, J. Källne, F. Reide, and N. Willis, Phys. Lett. 61B, 47 (1976).
[5]E. Auld *et al.*, Ref. 3, p. 21.
[6]N. S. Wahl, J. N. Craig, and D. Ezrow, Nucl. Phys. A268, 459 (1976).
[7]D. R. F. Cochran, P. N. Dean, P. A. M. Gram, E. A. Knapp, E. R. Martin, D. E. Nagle, R. B. Perkins, W. J. Schlaer, H. A. Thiessen, and E. D. Theriot, Phys. Rev. D 6, 3085 (1972).
[8]P. W. James, D. A. Bryman, G. R. Mason, L. P. Robertson, T. R. Witten, and J. S. Vincent, TRIUMF report, 1976 (unpublished).
[9]This work was supported in part by the National Science Foundation, the National Aeronautics and Space Administration, and the Commonwealth of Virginia.
[10]H. Brody, S. Frankel, W. Frati, D. Yang, C. F. Perdrisat, K. Z. O. Ziock, and J. C. Comiso, Phys. Lett. 71B, 79 (1977).
[11]J. B Cumming, J. Hudis, A. M. Poskanzer, and S. Kaufman, Phys. Rev. 128, 2392 (1962).
[12]W. Dollhopf, Ph.D. thesis, College of William and Mary, 1975 (unpublished).
[13]S. Frankel, W. Frati, O. Van Dyck, R. Werbeck, and V. Highland, Phys. Rev. Lett. 36, 642 (1976).
[14](a) S. Frankel, Phys. Rev. Lett. 38, 1338 (1977); (b) Phys. Rev. C 17, 694 (1978); (c) University of Pennsylvania, Report No. UPR 0087T, 1978 (unpublished).
[15]R. D. Amado and R. M. Woloshyn, Phys. Lett. 69B, 400 (1977).
[16]W. O. Lock and D. F. Measday, *Intermediate Energy Physics* (Methnen, London, 1970), p. 212.
[17]M. M. Block, Phys. Rev. 101, 796 (1956).
[18]G. Jones, contribution to the Second International Conference on the Nucleon-Nucleon Interaction, Vancouver, 1977 (unpublished).
[19]L. R. B. Elton, *Nuclear Size* (Oxford U.P., London,

1961), p. 31.
[20]I. J. McGee, Phys. Rev. 151, 772 (1966).
[21]M. M. Sternheim and R. R. Silbar, Phys. Rev. D 6, 3117 (1972); also D. A. Sparrow, M. M. Sternheim, and R. R Silbar, Phys. Rev. C 10, 2215 (1974).
[22]G. D. Harp, Phys. Rev. C 10, 2387 (1974).
[23]G. F. Bertsch, Phys. Rev. C 15, 713 (1977).